Polarization and high resolution parametric spectral analisys applied to the seismic signals recorded on the Marsili submarine volcano

A. D'Alessandro, G. D'Anna, D. Luzio, G. Mangano

Geological and geophysical setting

The rifting, which started during the Upper Oligocene in the area of the Southern Tyrrhenian, produced the Vavilov Basin (8.5-4.5 Ma) and the Marsili Basin (2.0-1.7 Ma) (*Fig. 1a*) that are marked by the two homonymous volcanoes (*Argnani, 2000*). The diachronous opening of the Marsili and Valilov Basins was related to a sharp acceleration of the roll-back of the Ionian Lithosphere subducting below the Southern Tyrrhenian Sea (*Gueguen et alii, 1998*).

The elongated Marsili Seamount has an altitude of 3000 m above the sea floor, and runs NNE-SSW for a approximately 60 km; it has a mean width of 16 km. This seamount is a back-arc volcano with a dominant tholeitic petrochemical affinity (*Trua et alii, 2004*).

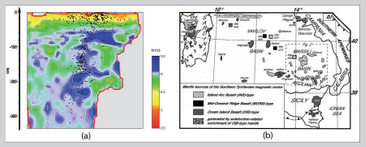

Fig. 1: *a) Schematic map of the Cenozoic magmatic rocks of the southern Tyrrhenian region modified by Trua et alii 2004 after Serri et alii, 2001; b) Vp section under Marsili basin; Earthquakes within 15 km of the sections are also plotted.*

Due to its position, the main geophysical features of the Marsili Basin are largely unknown. However, several authors have constructed models of the lithosphere of the Southern Tyrrhenian Basin, (*Marani et alii, 2004; Nicolosi et alii 2006; Montuori et alii 2007, Calò et alii, 2008*) which provide information about the Marsili Basin's role in the geodynamic evolution of the Tyrrhenian.

From the observation of the 3D model of the Marsili Basin, obtained by using a new LET inversion technique (*Calò et alii, 2008*) (a dataset composed of 28873 P and 9990 S arrival times and 78352 P and 26086 S differential times was employed), it can be seen that the vertical Vp, Vs and Vp/Vs seismic sections across the Basin show (*Fig. 1b*) two **low Vp and Vs and high Vp/Vs bodies under the Marsili** and Stromboli volcanoes, above the high velocity layer related to the upper part of the Ionian subducting slab.

Panza et alii (2004) estimated the 3D S-wave velocity model of the Southern Tyrrhenian lithosphere, by using a surface-wave tomography technique (*Pontevivo & Panza, 2002*). The relatively low velocity obtained in the uppermost mantle beneath Marsili was ascribed by the authors to the existence of large amounts of melt.

Mongelli et alii (1992) compiled a heat flow map of the Tyrrhenian Sea and the surrounding areas. This map shows a very high regional mean value of 120 mW m-2 with a **local maximum of 245 mW m-2 centred on Marsili**. This maximum was attributed to the recent tectonic and volcanic activity (*Mongelli et alii, 2004*).

Beccaluva et alii (1985) and Marani et alii (1999) collected some rock samples from the Marsili Basin that had undergone a strong degree of hydrothermal alteration.

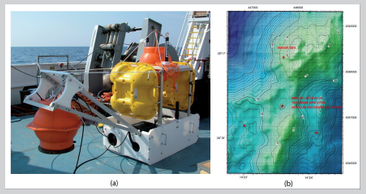

Fig. 2: *a) The New broadband OBS/H of INGV; b) map of Marsili with the deployment point.*

The experiment

In July 2006, in the framework of the PRO.ME.TH.E.US project, on board the ship Universitatis, a multi-disciplinary research was conducted in the area of the Marsili volcano. During this experiment the **INGV staff successfully deployed the prototype of a broadband OBS/H on Marsili's flat top at a depth of 790 m** (*Fig. 2a and 2b*). This equipment was developed under a project funded by an agreement between the *Italian National Civil Protection Department* (DPC) and INGV.

The OBS/H recorded for 9 days, from 12th to 21st July 2006 (*D'Anna et alii, 2007*). It was equipped with a **Nanometrics Trilium 40s 3C velocimeter** and an **OAS E-2PD hydrophone**. The OBS/H has an auto-leveling system. The azimuthal orientation of the horizontal components of the seismic sensor, initially unknown, was statistically determined by polarization analysis of well localized seismic events.

Tectonic events

Different types of seismic events, probably related to tectonic and volcanic activity, were observed on the entire record. **The OBS/H recorded 19 tectonic events: 8 regional events, 1 teleseismic event and 10 small local events.**

The regional events were located by INGV (*Fig 3b*) while the teleseismic event was the M=7.2 earthquake that took place on Java on 17th July 2006 (fig. 3a).

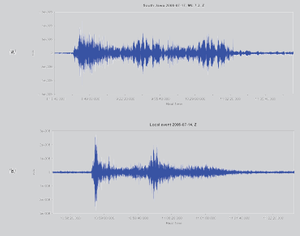

Fig. 3: *Vertical component of (a) Jawa event of 2006/07/17, M=7.2 and (b) a local earthquake.*

The regional events were used to estimate the azimuthal orientation of the seismometer through polarization analysis. We compared the known back azimuth of the located events with the back azimuth determined by polarization analysis of the P-wave arrivals recorded by the OBS/H. The sensor orientation was thus determined by linear regression between the back azimuth located by INGV (y) and the one (x) computed using the equation y=x+q (fig. 4a-4b). The correction estimated was equal to +144.7° with a probable error of 18.57°.

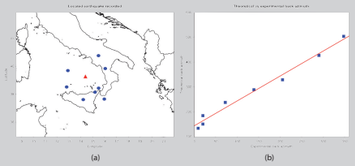

Fig. 4: *(a) Map of the located regional earthquakes and (b) linear regression between theoretical and experimental back-azimuth.*

Seismic noise and volcanic tremor

To compare the acceleration Power Spectral Density (PSD) of the noise recorded on Marsili with both Peterson's (1993) land High Noise Model (HNM) and Low Noise Model (LNM), we transformed the 40-hours velocity record into acceleration.

In order to calculate the PSD of this signal we applied the periodogram averaging method. To this end we divided the signal into 80 s intervals (16000 samples) with an overlap of 40 s, applied a Hanning window to each interval and used the FFT.

Fig. 5b shows the most significant differences between Peterson's PSD and the Marsili one. The very high noise level at low frequency is probably to be referred to the large scale sea currents or low-frequency sea waves. The double spectral peak near 0.2 Hz was caused by sea waves

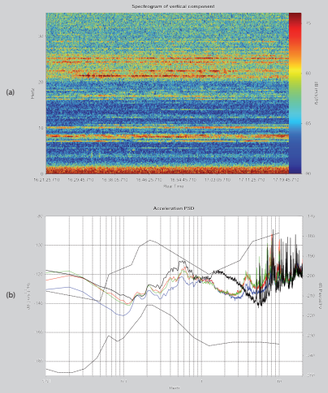

Fig. 5: *(a) Example of spectrogram of one hour of vertical component seismic noise and (b) acceleration PSD of seismic and hydroacoustic noise recorded on Marsili.*

that mostly propagate as the fundamental mode of the Rayleigh waves (*Webb, 1998*) while the peak at about 0.6 Hz could be imputed to interference by sea waves. Moreover, the ocean seismic noise on Marsili shows a very high power level, above 5 Hz; this noise level is mostly controlled by wave breaking and man-made sources. **The stable peak at about 3.8 Hz is probably associated to volcanic activity.** This frequency coincides with the main frequency band of VT-B events (see the following sections). Therefore, **this noise component could consist of a sequence of low-energy events with inter-event intervals of a few seconds**.

The PSD pressure signal of the Hydrophone does not show significant morphological differences in respect of the acceleration PSD (except in the range 1 - 4 Hz).

In order to analyze the time variations in the frequency content of the noise, we calculated the short time Fourier transform, with sliding windows of 10 seconds (2000 samples). The main peaks were characterized by nearly constant frequency and amplitude.

To better understand the nature of the seismic noise recorded on Marsili, we applied a **time-frequency polarization analysis** to the vectorial signal. The information contained in the Fourier spectra of the 3 components can be expressed as a function of the geometric elements of the polarization ellipse of each vectorial harmonic component versus frequency. The geometrical elements thus determined are the length of the major and minor axes, the strike and dip of each ellipse plane. The time variation of these functions was also determined by using a translating analysis window.

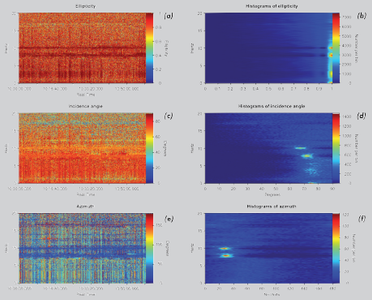

Fig. 6: *time-frequency distribution of the polarization attributes (6a = ellipticty, 6c = incidence angle, 6e = azimuth) and relative histograms (6b, 6d, 6f)*

Fig. 6 shows the time-frequency distribution of the polarization attributes (6a = ellipticty, 6c = incidence angle, 6e = azimuth) and relative histograms (6b, 6d, 6f). *Fig. 6* also shows that the components having a 3.8, 7.5, 10 Hz frequency, and some others, nearly always have a linear polarization. The same components often have high incidence angles (near horizontal) and azimuths of about 30°. These seismic noise components have sources that are similar to those of VT-B events , which will be described in the next section.

Volcano-tectonic events

817 events recorded on Marsili were classified as B-type Volcano-Tectonic events (VT-B); *Fig. 7* shows an example of a VT-B (filtered in the band 2.0 and 7.0 Hz), while *Fig. 8* shows a one-hour record and its amplitude spectrogram containing a VT-B swarm.

Time analysis shows that the VT-B events had **emergent low-energy** P-wave onsets and a mean duration of 30 s whereas they often **do not show any clear S-wave arrival**. Instead, the spectral analysis shows that the seismic energy of the VT-B events was mainly concentrated in the narrow frequency band 1.5 - 7 Hz, with the maximum at about 3.8 Hz.

Furthermore, we applied a polarization analysis to the filtered signals. To improve the estimates of the polarization attributes, the covariance matrix was corrected for the presence of noise and its stocasticity and stationarity were assumed. The polarization analysis was applied to more than 200 VT-B with high energy, to determine the P-wave horizontal component of the polarization vector and, thus, the back-azimuth.

Fig. 9 shows the vertical component of a VT-B and its polarization attributes. A **high degree of linearity** is clear in the first part of the trace where the body waves are dominant. The azimuth and incidence angle show only a few time variations. As stated before, we believe that the VT-B events are made up of body waves coming from shallow sources.

Fig. 10 shows the **rose diagram of the estimated back-azimuth of the 220 VT-B analyzed**. It clearly displays two main directions in the NE quadrant, probably to be referred to the presence of two distinct seismogenetic areas.

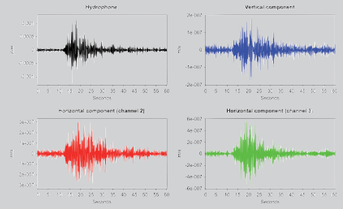

Fig. 7: *Example of a VT-B event (filtered in the band beetween 2.0 and 7.0 Hz).*

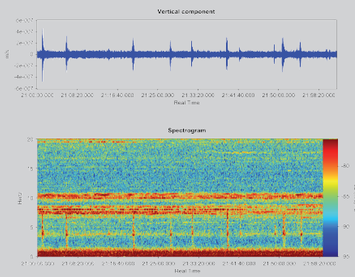

Fig. 8: *One hour of recording and its amplitude spectrogram containing a VT-B swarm.*

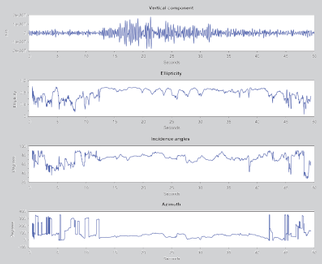

Fig. 9: *Vertical component of a VT-B event and the its polarization attributes.*

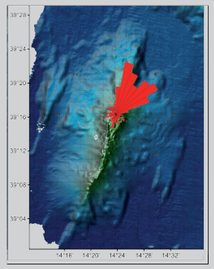

Fig. 10: *Rose diagram of the estimated azimuth of the 220 VT-B analyzed.*

Short duration events

36 events were also recorded on the Marsili volcano that show the rapid decaying trend of a quasi-monochromatic wave (*Fig. 11*). Similar waveforms are often recorded in volcanic and hydrothermal areas. These were attributed to events called Tornillo or LPE (Long Period Event) or Crack-Event or **SDE (Short Duration Event)** depending on their spectral content and damping characteristics. Such events are generated by oscillations of a resonant body excited by magmatic or hydrothermal activity (*Chouet, 1996*).

A number of models have been proposed for this type of event to explain the waveforms and dominant frequencies: rapid discharges of gas (*Steinberg and Steinberg, 1975*), oscillations of magma-filled cracks excited by crack tip extension (*Chouet, 1981, 1986, 1988*), resonance of a magma pipe (*Chouet, 1985*), oscillations of a spherical magma reservoir (*Crosson and Bame, 1985; Fujita et alii, 1995*), periodic magma flow (*Ukawa and Ohtake, 1987*), acoustic emissions from collapsing bubbles (*Chouet, 1992*), self-excitation of a magma conduit in a manner similar to that of a flute (*Julian, 1994*) and oscillations of a steam-filled crack by unsteady choked flow (*Morrissey and Chouet, 1997*).

Nakano et alii (1998) model the SDE as a transient wave excited by the eigenoscillations of a resonator that has a finite length scale embedded in a homogeneous elastic infinite medium. The evaluation of this typical complex frequency allows you to determine some properties of the source.

The method that we applied is based on an **inhomogeneous autoregressive model of a linear dynamic system**, in which the excitation is assumed to be a time-localized function applied at the beginning of the event (*Nakano et alii, 1998*). The Sompi method, that uses the tail of an exponential decaying harmonic waveform, was employed to determine the characteristic complex frequency of the event.

The parametric spectral analysis of the SDE signals provided reliable estimates of their dominant complex frequencies. Plotting them on the complex frequencies plane (*Fig. 12*) **we identified two distinct clusters that had mean complex frequencies f=7.8s−1, g=-0.35s−1 and f=7.5s−1, g=-0.47s−1 respectively**. These two clusters are probably linked to two different seismogenetic volumes.

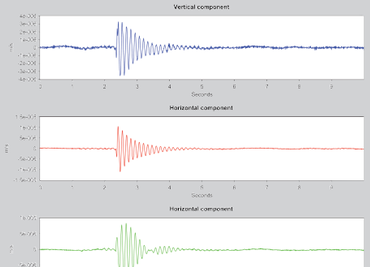

Fig. 11: *Example of SDE recorded on Marsili volcano.*

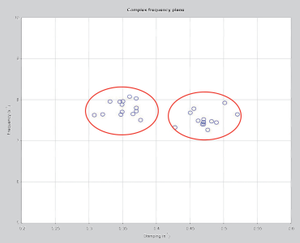

Fig. 12: *Plotting of the SDE complex frequecies estimated by Sompi method.*

Argnani, A. (2000), The southern Tyrrhenian subduction system: Recent evolution and neotectonic implications, Ann. Geophys., 43, 585–607.

Beccaluva L., Rossi P. L. & Serri G. (1982) – Neogene to Recent volcanism of the Southern Tyrrhenian-Sicilian area: Implications for the geodynamic evolution of the Calabrian arc. Earth Evolutionary Sciences, 3: 222-238.

Chouet B. (1996) – New methods and future trends in seismological volcano monitoring. Monitoring and Mitigation of Volcano Hazards, Eds. R. Scarpa and R. Tilling, Springer-Verlag, Berlin New York: 23-98.

D'Anna G., Mangano G. , D'Alessandro A., Amato A. (2007) - The new INGV broadband OBS/H: test results on submarine volcano Marsili and future developments. Geophysical Research Abstracts, Vol. 9, 06583.

Gueguen E., Doglioni C. & Fernandez M. (1998) – On the post-25 Ma geodynamic evolution of the western Mediterranean. Tectonophysics, 298: 259-269.

Marani M.P, Gamberi F., Casoni L., Carrara G., Landuzzi V., Musacchio M., Penitenti D., Rossi L. & Trua T. (1999) – New rock and hydrotermal samples from the southern Tyrrhenian sea: the MAR-98 research cruise. Giornale di Geologia, 61: 3-24.

Marani M.P. (2004) – Super-inflation of a spreading ridge through vertical accretion. Mem. Descr. Carta Geol. d'It., LXIV: 185-194.

Mongelli F., Zito G., De Lorenzo S., Doglioni C. (2004) – Geodynamic interpretation of the heat flow in the Tyrrhenian Sea. Mem. Descr. Carta Geol. d'It., LXIV: 71-82.

Mongelli, F., Cataldi R., Celati R., Della Vedova B., Fanelli M., Nuti S., Pellis G., Squarci P., Taffi L. & Zito G. (1992) – Geothermal regime in Italy, in Italian Working Group for the Geothermal Atlas in Europe, <<Geothermal Atlas of Europe>> edited by E. Hurting, Čermák V., Haenel R. and Zui V. (H.Haack Verlagsges., Gotha), 54-59.

Montuori C., Cimini g. B. & Favali P. (2007) – Teleseismic tomography of the southern Tyrrhenian subduction zone: New results from seafloor and land recordings. J. Geophys. Res., vol. 112: B03311.

Nicolosi I., Speranza F. & Chiappini M. (2006) - Ultrafast oceanic spreading of the Marsili Basin, southern Tyrrhenian Sea: Evidence from magnetic anomaly analysis. Geology; September 2006; v. 34; no. 9; p. 717-720;

Panza G.F., Pontevivo A., Saraò A., Aoudia A., Peccerillo A. (2004) – Structure of the lithospher-asthenosphere and volcanism in the Tyrrhenian Sea and surroundings. Mem. Descr. Carta Geol. d'It., LXIV: 29-57.

Peterson J. (1993) – Observation and modeling of background seismic noise: U.S. Geol. Surv. Open-File rept., Albuquerque, 93-322.

Pontevivo A. & Panza G.F. (2002) – Group Velocity Tomography and Regionalization in Italy and bordering areas. Phys. Earth Planet. Inter., 134: 1-15.

Trua T., Serri G., Rossi P.L. (2004) – Coexistence of IAB-type and OIB-type magmas in the southern Tyrrhenian back-arck basin: evidence from recent seafloor sampling and geodynamic implications. Mem. Descr. Carta Geol. d'It., LXIV: 83-96.

Webb S.C. (1998) – Broadband seismology and noise under the ocean. Reviews of Geophysics, 36, 1: 105-142.

Istituto Nazionale di Geofisica e Vulcanologia
Centro Nazionale Terremoti

OBS Lab Gibilmanna
obslab@ingv.it